Arginine-rich cell-penetrating peptides induce membrane multilamellarity and subsequently enter via formation of a fusion pore

Christoph Allolio[a,b,c,d,1], Aniket Magarkar[a,e,1], Piotr Jurkiewicz[f], Katarína Baxová[a], Matti Javanainen[a], Philip E. Mason[a], Radek Šachl[f], Marek Cebecauer[f], Martin Hof[f], Dominik Horinek[b], Veronika Heinz[g], Reinhard Rachel[h], Christine M. Ziegler[g,i], Adam Schröfel[j], and Pavel Jungwirth[a,2]

[a]Institute of Organic Chemistry and Biochemistry, Czech Academy of Sciences, CZ-166 10 Prague 6, Czech Republic; [b]Institute of Physical and Theoretical Chemistry, University of Regensburg, D-93040 Regensburg, Germany; [c]Fritz Haber Research Center, The Hebrew University of Jerusalem, Jerusalem 9190401, Israel; [d]Department of Chemistry, The Hebrew University of Jerusalem, Jerusalem 9190401, Israel; [e]Faculty of Pharmacy, University of Helsinki, Helsinki 00014, Finland; [f]J. Heyrovský Institute of Physical Chemistry, Czech Academy of Sciences, 182 23 Prague 8, Czech Republic; [g]Institute of Biophysics and Biophysical Chemistry, University of Regensburg, D-93040 Regensburg, Germany; [h]Microbiology and Archaea Centre, University of Regensburg, D-93040 Regensburg, Germany; [i]Institute of Biophysics and Biophysical Chemistry, University of Regensburg, D-93040 Regensburg, Germany; and [j]Imaging Methods Core Facility at Biocev, Faculty of Sciences, Charles University, 242 50 Vestec, Czech Republic

Edited by Michael L. Klein, Temple University, Philadelphia, PA, and approved October 10, 2018 (received for review July 6, 2018)

Arginine-rich cell-penetrating peptides do not enter cells by directly passing through a lipid membrane; they instead passively enter vesicles and live cells by inducing membrane multilamellarity and fusion. The molecular picture of this penetration mode, which differs qualitatively from the previously proposed direct mechanism, is provided by molecular dynamics simulations. The kinetics of vesicle agglomeration and fusion by an iconic cell-penetrating peptide—nonaarginine—are documented via real-time fluorescence techniques, while the induction of multilamellar phases in vesicles and live cells is demonstrated by a combination of electron and fluorescence microscopies. This concert of experiments and simulations reveals that the identified passive cell penetration mechanism bears analogy to vesicle fusion induced by calcium ions, indicating that the two processes may share a common mechanistic origin.

cell-penetrating peptide | membrane fusion | fluorescence microscopy | electron microscopy | molecular dynamics

Cell-penetrating peptides have a unique potential for targeted drug delivery; therefore, mechanistic understanding of their membrane action has been sought since their discovery over 20 y ago (1). While ATP-driven endocytosis is known to play a major role in their internalization (2), there has been also ample evidence for the importance of passive translocation (3–5) for which the direct mechanism, where the peptide is thought to directly pass through the membrane via a temporary pore, has been widely advocated (4, 6–8). Here, we question this view and show that arginine-rich cell-penetrating peptides instead passively enter vesicles and live cells by inducing membrane multilamellarity and fusion.

Ions do not dissolve in oil. From this point of view the direct passive mechanism of cell penetration is intuitively problematic, as cationic peptides such as polyarginines or the transactivating transcriptional activator (TAT) are too highly charged to be able to pass through the "oily" interior of a lipid membrane. The concept of direct penetration was seen plausible due to the action of the related antimicrobial peptides, which are also charged, but in addition contain a large fraction of hydrophobic residues (9): These peptides are known to stabilize pores in membranes (10). At a close inspection, however, it becomes clear that their charged side chains do not interact directly with the aliphatic chains in the low dielectric interior of the phospholipid bilayer, but rather stabilize transient water channels or act as terminal residues anchoring the transmembrane helix (9). Taken together, the passive action of cell-penetrating peptides (CPPs) seems to be very different from direct translocation across an otherwise unperturbed cell membrane.

To make matters even more confusing, experimental facts and suggested mechanisms often seem contradictory to each other. For example, there are conflicting reports whether or not nonaarginine (R_9) is able to penetrate vesicles composed purely of 1-palmitoyl-2-oleoyl-phosphatidylcholine (POPC) (5, 11, 12). Additionally, fluorescence microscopy suggests that R_9 is able to deform membranes (5, 13) and small-angle X-ray scattering (SAXS) experiments reveal phase transitions induced in lipid systems by polyarginines (4). An important factor in these observations appears to be the membrane composition with negatively charged lipids facilitating membrane translocation of cationic peptides (7, 14). Indeed, there is some evidence that a direct mechanism may be enabled by hydrophobic counterions, such as pyrene butyrate (12, 15) or presence of an unphysiological concentration of phosphatidic acids (7). The relevance to of these phenomena to actual cellular uptake is not clear, so that current discussions present direct mechanisms side by side with endocytosis-like membrane deformations induced by the CPPs (16).

Another fundamental cellular process involving membranes and charged species is fusion of vesicles with the cell membrane during calcium-triggered exocytosis. In neuronal cells,

Significance

The passive translocation mechanism of arginine-rich cell-penetrating peptides has puzzled the scientific community for more than 20 y. In this study we propose a hitherto unrecognized mechanism of passive cell entry involving fusion of multilamellar structures generated by the cell-penetrating peptides. The geometry of entry for this mechanism is completely different from previously suggested direct translocation mechanisms, leading to another paradigm for designing molecular carriers for drug delivery to the cell.

Author contributions: C.A., A.M., and P. Jungwirth designed research; C.A., A.M., P. Jurkiewicz, K.B., M.J., P.E.M., R.S., M.C., D.H., V.H., R.R., C.M.Z., and A.S. performed research; P.E.M., M.H., V.H., R.R., and P. Jungwirth analyzed data; and C.A. and P. Jungwirth wrote the paper.

The authors declare no conflict of interest.

This article is a PNAS Direct Submission.

[1]C.A. and A.M. contributed equally to this work.

[2]To whom correspondence should be addressed. Email: pavel.jungwirth@uochb.cas.cz.

This article contains supporting information online at www.pnas.org/lookup/suppl/doi:10.1073/pnas.1811520115/-/DCSupplemental.

Published online November 5, 2018.

vesicle–membrane fusion is mediated by the SNARE protein complex (17, 18) with synaptotagmins (19); nevertheless, it can also be induced in in vitro lipid vesicles without the need for the presence of the protein machinery (20, 21). It is experimentally well established that Ca^{2+} is a key player capable of promoting vesicle fusion (22) and there is general consensus about the fusion mechanism, which proceeds via a stalk intermediate, followed by formation of a hemifused structure and opening of a fusion pore (23, 24). In this context, it is worth mentioning that cationic CPPs, especially TAT and its derivatives, are known to aggregate at phospholipid membranes and occasionally fuse vesicles (2, 5, 20, 25). This brings up the idea, which is examined further in this study, that the processes of passive cell penetration and membrane fusion may be mechanistically more intimately connected than thought so far (25).

Results and Discussion

Exploring Vesicle Penetration by a Fluorescence Leakage Assay. To explore the potential connection between cell penetration and membrane fusion, we start by investigating the abilities of R_9 as an archetypal CPP, in contrast to non-CPPs like tetraarginine (R_4) or nonalysine (26) (K_9), to penetrate and cause leakage of large unilamellar vesicles (LUVs) of varying lipid compositions using a fluorescence leakage assay (for details see *Materials and Methods* and *SI Appendix*). While, contrary to some published data (12), pure POPC LUVs do not show leakage upon exposure to R_9 even at high peptide concentrations, LUVs composed of mixtures of 1,2-dioleoyl-phosphatidylethanolamine (DOPE) and 1,2-dioleoyl-phosphatidylserine (DOPS) exhibit leakage as long as the content of DOPE is sufficiently high (*SI Appendix*, Table S3). Despite different lipid composition of the present vesicles compared with live cells, we did recover the arginine "magic," i.e., the high activity of CPPs with more than about 7 amino acids and high arginine content (27). In these vesicles, similar to experiments in cells, R_9 was always found to be a more efficient leakage agent than K_9 and the essentially inactive R_4 peptide (Fig. 1, *Top Left*). Using dynamic light scattering (DLS) measurements we showed that leakage is accompanied with vesicle aggregation, as the leakage kinetics mimic the increase in time of the mean diameter of the aggregates (see Fig. 1, *Top Right* and *SI Appendix*, Table S3 for the DOPE-rich lipid composition).

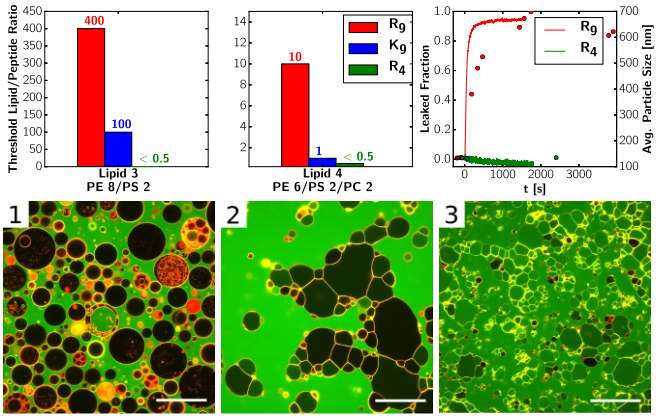

Fig. 1. Fluorescence spectroscopy results. (*Top Left* and *Top Center*) Threshold concentrations for leakage induced by R_9, K_9, and R_4 given as inverse of the peptide/lipid ratios for two lipid compositions: DOPE/DOPS 80/20 (lipid 3) and DOPE/DOPC/DOPS 60/20/20 (lipid 4) (the higher the threshold value, the more efficient the peptide is in leaking the vesicles). (*Top Right*) DLS measurements showing particle growth (right axis, solid circles) overlaid with leakage kinetics (left axis, lines) for R_9 for composition 3 and absence of particle growth and leakage for R_4. (*Bottom*) Fluorescence microscopy images showing the effect of R_9 on GUV with composition 4. From *Left* to *Right*: 1, no peptide added; 2, shortly after addition of R_9; and 3, final state after 1 h. (Scale bars, 50 μm.)

Membrane Fusion Induced by Calcium As Well As by Cationic Cell-Penetrating Peptides. The range of lipid compositions of vesicles capable of being leaked by R_9 is at odds with simulations of direct translocation, where a far higher translocation free energy has been predicted for DOPE-rich bilayers than for those rich in POPC (28). However, it seems to match compositions known to enhance vesicle fusion by calcium (20, 21, 29). Both phosphatidylethanolamine (PE) and phosphatidylserine (PS) (as well as several other anionic lipids) are fusogenic in presence of Ca^{2+} (30–32). To verify this correlation, we repeated the experiments with Ca^{2+} instead of R_9. Indeed, we were able to observe calcium-induced leakage for lipid compositions that were most susceptible to leakage by the CPPs as well (*SI Appendix*, Table S3). To obtain a comparable effect, however, the concentration of Ca^{2+} had to be significantly higher than that of R_9, even when taking into account the significantly larger charge carried by the latter species.

At high peptide content, the LUV leakage kinetics are described quantitatively by a second-order rate law in the vesicle concentration (for details see *SI Appendix*, Fig. S11 and the kinetic model in *SI Appendix*). This indicates that aggregation of vesicles and the double bilayer formed during this process is essential for vesicle leakage. It is revealing that for all lipid compositions at which significant leakage occurs the vesicles also exhibit R_9-induced fusion, as detected by a near complete lipid mixing in a Förster resonance energy transfer (FRET) assay (*SI Appendix* and *SI Appendix*, Fig. S11). Moreover, the leaky lipid compositions are those known to be susceptible to Ca^{2+}-mediated fusion. Note that leaky fusion has been observed previously in conjunction with CPPs and has even been used to classify them (25). In addition to the above circumstantial evidence for a direct connection between cell penetration and membrane fusion we add further experimental support using confocal microscopy, finding agglomeration of giant unilamellar vesicles (GUVs) together with leakage (Fig. 1). We were able to observe fusion of GUVs directly (*SI Appendix*, Movie S1) and, using Oregon Green 488 (OG)-labeled peptides, we confirmed a preferential adsorption of fluorescently labeled R_9 to the vesicles (*SI Appendix*, Fig. S8). Finally, adding Ca^{2+} instead of R_9 to the GUVs, we found a functionally analogous behavior (*SI Appendix*, Fig. S8).

Ideal Fusion Topologically Precludes Cell Penetration. The similarities in aggregation/fusion caused by R_9 and Ca^{2+} are illustrated in Fig. 2 *A*–*J*. In the context of the present study, it is important to note that there is no topological way for peptides to enter the vesicles from the outside (or do the reverse) by an ideal fusion process, within which two unilamellar vesicular structures coalesce, as it merely connects the interiors of the two vesicles. A previous electron microscopy study of Ca^{2+}-mediated fusion reported content loss along the fusion diaphragm, attributing it to the strain induced by the deformation during agglomeration (33). A close observation of the GUVs in Fig. 1 indeed reveals that they are significantly deformed as the agglomeration creates nearly planar surfaces at the regions of contact, indicating high tension. While tension supports several fusion steps (34), the large surface tension of the agglomerated, flat, and fusing double bilayers can also lead to rupture—depending on the initial tension of the vesicles it may overcome the line tension leading to a membrane pore. However, a small, transient, pore near the fusion stalk can hardly be the main mechanism of penetration of peptides into vesicles since it will rapidly close (35, 36), making it hard for cargo to pass through. Such pores are also associated with positive curvature, as induced by certain amphipathic helices (37), whereas here we stabilize fusion stalk and pore with

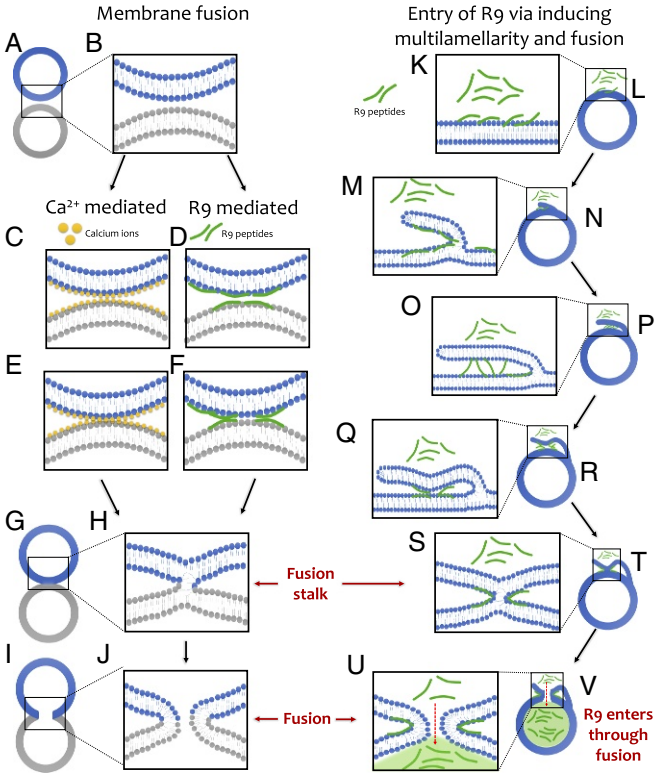

Fig. 2. The schematic mechanisms of R_9- and Ca^{2+}-mediated vesicle fusion. (*A* and *B*) Fusion of different vesicles (in blue and gray) (*A*), by interface contact (*B*). (*C* and *D*) Adsorption of the charged particles (R_9 in green and Ca^{2+} in yellow). (*E* and *F*) Agglomeration of the bilayers induced by cross-linking. (*G*) Stalk formation. (*H*) Opening of the fusion pore. (*I* and *J*) R_9 translocation via self-fusion of a single vesicle, (*K*–*V*) starting from a flat vesicle surface bilayer. (*K*) Strong adsorption of R_9. (*K* and *L*) Membrane bifurcation through adhesion and curvature. (*M*–*P*) Extension of the bifurcated bilayer (*M* and *N*) through R_9 cross-linking (*O* and *P*). (*Q* and *R*) Agglomeration of the bilayers induced by cross-linking of two bilayers on the same vesicle. (*S*–*V*) Stalk formation (*S* and *T*) and opening of the fusion pore through which additional R_9 peptides enter (*U* and *V*).

negative curvature inducing PE lipids (23) and the hydrophilic R_9. For a cell membrane to be ruptured at the fusion diaphragm, a large enough membrane fold would have to be generated first. This is possible only for a system without a large surface tension. However, such membranes are unlikely to be ruptured by a fusion event. Therefore, rupture cannot explain continuous leakage into intact vesicles, nor is it a plausible mechanism for cell penetration as cells tightly regulate their inner pressure and membrane tension and are rich in cholesterol, which increases pore line tension. We show below that a solution lies in locally bifurcating the membrane, leading to multilamellar structures. Such a pathway allows the peptides to enter by fusion without having to form transient pores, as shown schematically in Fig. 2 *K*–*V*.

Induced Multilamellarity as a Solution to the Topological Conundrum Observed by Cryoelectron Microscopy: Seeing Is Believing. A tendency of GUVs (13) or cells (12) to become multilamellar upon addition of CPPs has been observed recently. To further explore this idea, we first conducted cryoelectron microscopy (cryo-EM) experiments on LUVs. The obtained cryo-EM images indeed reveal formation of multilamellar domains and lipid bilayer bifurcations after the addition of R_9 (Fig. 3). Additional time-resolved FRET experiments on fluorescently labeled LUVs reveal presence of interbilayer energy transfer, which provides independent confirmation for the induction of multilamellar lipid structures by R_9 (*SI Appendix* and *SI Appendix*, Fig. S11). Importantly, Ca^{2+} ions are also able to fuse and collapse vesicles to multilamellar phases due to the ability of Ca^{2+} to bridge phosphates from different bilayers (33). The cryo-EM structures also provide some additional evidence for fusion, as the LUVs in Fig. 3*A* are many times larger than those found in the initial state (*SI Appendix*, Fig. S7*A*).

Multilamellar structures can be formed via folding of a membrane or by stacking of deflated vesicles. Any process based on direct membrane stacking would, however, add an even number of bilayers in between the vesicles and, therefore, would not lead to leakage via fusion. It is thus a key finding that by counting the lipid bilayers we frequently find odd numbers (Fig. 3*D*). Moreover, a close inspection of the EM micrographs provides direct evidence for bilayer bifurcation at multiple positions (see Fig. 3*C* for an example). We conclude that R_9 is indeed capable of inducing multilamellarity by membrane adsorption and bifurcation, rendering a cell penetration mechanism via fusion feasible.

The proposed mechanism shares some similarities with the reverse micelle mechanism, proposed in the literature (38, 39). This mechanism also necessitates a small bifurcation, before the membrane edge is closed by forming the reverse micelle. The reverse micelle has negative curvature on the inside and is, therefore, stabilized by similar interactions to those of the bifurcations. We argue that the membrane edge energy can be compensated through extension of stable cross-linked multilamellar domains as seen in the EM pictures. In *SI Appendix* we show simulations, which indicate the stabilization of the bifurcation by R_9, but not R_4 even in the absence of cross-linking. The opening of a reverse micelle removes negative curvature from the system. In contrast to this, the fusion stalk (23) and pore both maintain a negative curvature—a finite bilayer thickness translates negative Gaussian curvature into negative mean curvature, present on both membrane leaflets (40). Thereby the whole mechanism can be driven by the same preferential interaction with R_9.

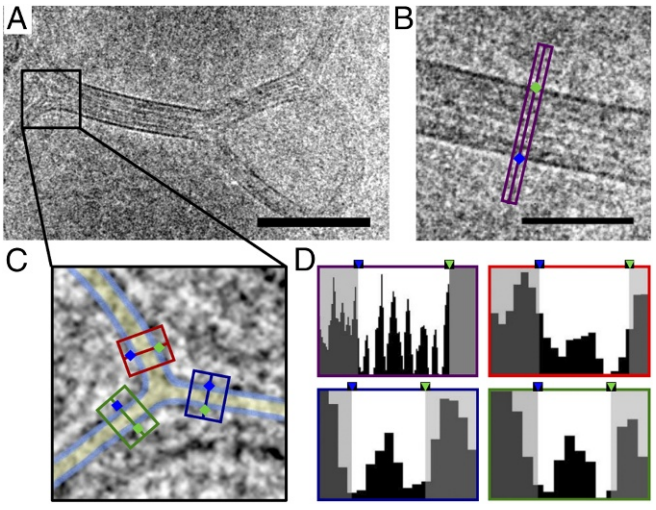

Fig. 3. Electron micrographs of LUVs in the presence of R_9. (*A*) Vesicles treated with R_9 (>60 s) fuse with each other and exhibit bifurcated, multilamellar membranes. (Scale bar, 100 nm.) (*B*) Example of a multilamellar membrane. (Scale bar, 50 nm.) The violet box is analyzed in *D*. (*C*) Example of a membrane bifurcation. The membranes before and after the bifurcation site are analyzed by line scans. The line-scan areas are marked with colored boxes. (*D*) The histograms are boxed in the same color as the respective line-scan areas in *B* and *C*. (*D*, *Top Left*) The histogram corresponding to the multilamellar membrane (shown in *B*) exhibits seven distinct minima attributed to individual membranes.

Fluorescence and EM on HeLa Cells. To directly explore the mechanism behind cellular uptake of CPPs in the absence of endocytosis, we first observed penetration into living human HeLa cells by fluorescence confocal microscopy (*SI Appendix*, Figs. S9 and S10). HeLa cells incubated with 15 μM OG-labeled R_9 peptide for 3 min at 4 °C already exhibited surface fluorescence and, in particular, the presence of highly fluorescent foci (*SI Appendix*, Fig. S9, arrows). Longer incubation of cells with the peptide increased the number of foci detected on HeLa cells. Cytosolic presence of the peptide was observed as soon as 5 min after addition of the peptide to the cells and the number of penetrated cells increased over prolonged incubation time (even when cells were washed after 3 min to remove free peptide from incubation medium). All cells with cytosolic peptide exhibited at least one to two fluorescent foci on their surfaces. Moreover, these foci were found only in cells with endocytosis blocked by low temperature.

These results suggest that R_9 rapidly accumulates in very few places on a cell at low temperatures. Previously, EM on cells revealed that addition of R_9 leads to the formation of layered membrane domains (41). Motivated by these observations, we performed EM experiments on HeLa cells with added fluorescently labeled R_9. In accord with our observations on vesicles and with previous EM on cells (41) we see regions of protrusions, bifurcations, and multilamellarity by incubating cells with R_9 at 4 °C. At these conditions active endocytosis is switched off and only passive cell penetration is operational (Fig. 4*B*). The branched structures (zoomed-in images in Fig. 4*C*) are topologically identical to those suggested in the schematic drawing in Fig. 2*M* and to the structures observed in the LUVs (Fig. 3). The observed protrusions indicate that a strong curvature-generating interaction is at work, as can be seen in Fig. 4*D*. Specifically, we interpret the budding spherical protrusions as being due to negative (Gaussian) curvature generation, similar to those occurring in a fusion stalk. By overlaying fluorescence images with EM we clearly see that the changes in the bilayer structure correlate with the location of the fluorescently labeled OG-R_9, as can be seen in Fig. 4*A*. Our EM images on HeLa cells are thus consistent with the above results on vesicles, as well as with previous observations showing that giant plasma membrane vesicles (GPMVs) are susceptible to R_9 penetration, but only in the presence of intact membrane proteins (3). Note that in contrast to our leakage experiments on LUVs the local, encapsulated foci will allow only very limited diffusion, thereby limiting potential cell toxicity of the CPPs. Their locality at the cell membrane also points to a yet unknown specific interaction which is not present in the synthetic vesicle systems.

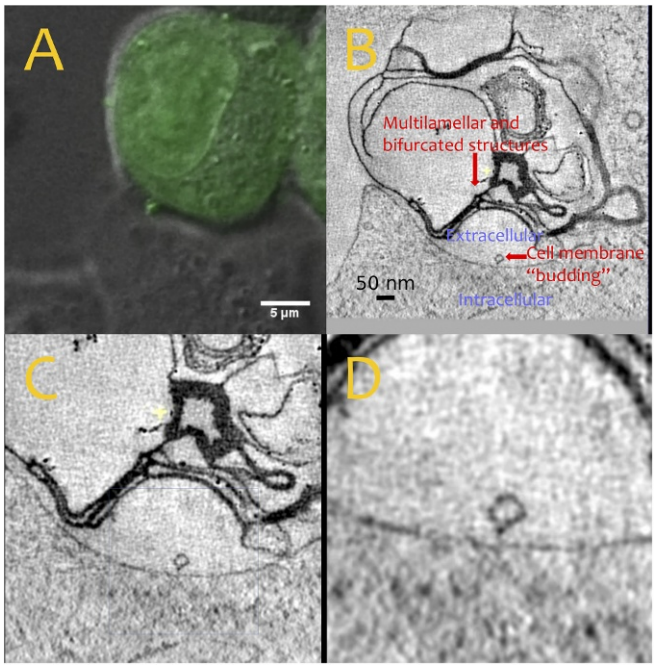

Fig. 4. EM and fluorescence microscopy images of the same spot on a fixated HeLa cell in the presence of OG-R_9. (*A*) A fluorescence microscopy image of the multilamellar spot showing the presence of the labeled peptide. (*B–D*) An EM image at three zoom-ins exhibiting bifurcated, multilamellar membranes and vesicle budding. (*C*) An example of a multilamellar membrane structure. (*D*) Focus on a budding protrusion.

Molecular Dynamics Simulations: Atomistic Insights. To gain atomistic insight into the fusion process and its connection to cell penetration we performed molecular dynamics simulations. Previous studies, based on continuum and coarse-grained models, agree that fusion proceeds via a stalk intermediate (23, 35). The stalk is strongly concave, explaining the observed lipid selectivity toward small (PE) headgroups as these stabilize negative curvature.

Our simulation setups involve strongly positively curved bilayer geometries, intended to lower the barriers for fusion (42, 43). The stress hereby induced in the PE-rich bilayers leads to spontaneous stalk formation in our simulations (see *Materials and Methods* and *SI Appendix* for full details). Snapshots from the R_9- or Ca^{2+}-mediated fusion processes are presented in Fig. 5. We find both Ca^{2+} ions and the charged R_9 side chains bind to lipid headgroups, primarily at the negatively charged phosphates. Subsequently, we observe mechanistic similarities in the membrane fusion mediated by Ca^{2+} and R_9. The first step in the fusion process is cross-linking, i.e., simultaneous binding of lipids from two membrane bilayers by either Ca^{2+} or R_9, with the latter found to be a particularly effective cross-linker. As the ions keep the bilayers in close contact, the lipid tails eventually cross-link, too, in what appears to be the rate-determining step of the whole fusion process. This lipid tail cross-linking occurs within about 0.5 μs. Once a cross-linking lipid tail has flip-flopped into the opposing bilayer, the stalk starts forming within a few nanoseconds (Fig. 5 *B* and *C*).

In Fig. 5*D* we examine the action of R_9 on the membrane in close detail. First, we note the long-range cross-linking capability of R_9, which is likely to be responsible for its strongly agglomerating effect on vesicles and for stabilizing the multilamellar structures we find in EM. R_9 tends to be only partially adsorbed at the membrane and can thus easily reach across the interface and attach to the second bilayer. It is clear that for such a cross-linking a minimum chain length is necessary, which explains the inefficiency of R_4 in this respect (see also the control simulation data in *SI Appendix*, Fig. S3). In addition, R_9 also forms agglomerates when cross-linking the interfaces. It is known that R_9 binding to membranes is more cooperative than that of K_9 (44), making the former a much more efficient agent of membrane fusion and cell penetration than the latter. The attraction of R_9 to negatively charged lipids also leads to a lipid sorting effect, with phosphatidylserine lipids (Fig. 5*D*, orange) being accumulated next to the R_9 agglomerate. Electrostatics-based lipid sorting (involving, e.g., gangliosides) may contribute to the action in cells, membranes of which would otherwise not be sufficiently active. In Fig. 5*D*, *Right* we show that R_9 is preferentially adsorbed to regions of negative curvature (45) (marked by the color-coded surface), as this allows it to efficiently bind its side chains to lipid headgroups (marked in gold). Aggregation of headgroups increases membrane tension in the headgroup region and exposes hydrophobic patches (visible in all panels of Fig. 5*D*). The exposure of hydrophobic patches in turn lowers hydration repulsion. Once lipid tails from opposing bilayers are in contact, lipid flip-flop can readily occur, starting thus the

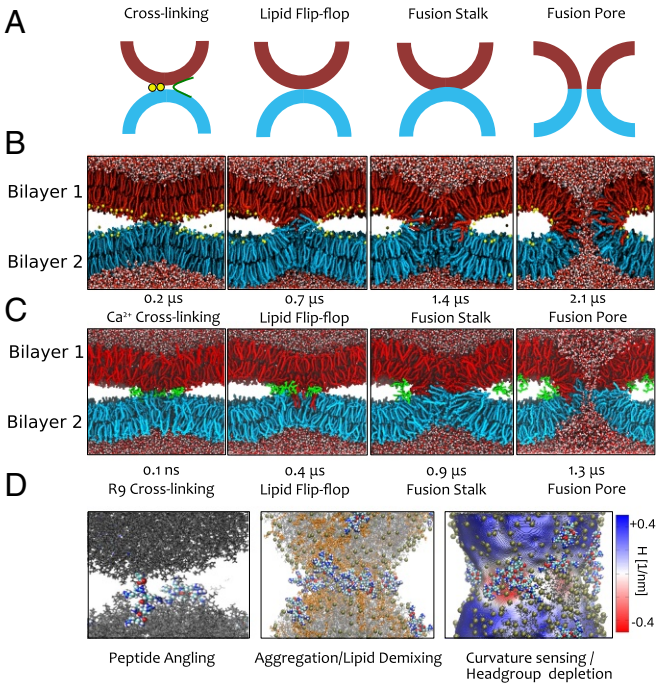

Fig. 5. (*A*) Schematic drawing of vesicle fusion–lipid cross-linking, stalk initialization, and subsequent onset of stalk formation through lipid flip-flop. (*B*) Time evolution of the Ca^{2+} fusing bilayer system. (*C*) Time evolution of the same system with R_9. (*C*, *Left* to *Right*) Cross-section of systems undergoing fusion: cross-linking, flip-flop, fusion stalk, and fusion pore. (*D*) Driving forces of the mechanism. Peptide "angling" cross-links vesicles and aggregates membranes, peptide agglomeration and lipid demixing create fusable interface, and negative curvature is generated through strong binding to headgroups.

fusion cascade. At the surface of the fusion stalk and the pore, a very strongly negative Gaussian curvature and a negative mean curvature occur simultaneously. This stabilizes the actual geometry and, therefore, lowers the barrier for fusion. The induction of negative Gaussian curvature was previously proposed as a characteristic of CPPs (4). Importantly for the present mechanism, we do not observe membrane rupture or water permeation during the fusion process.

Conclusions

In summary, we unraveled here a passive entry mechanism of CPPs via branching and layering of membranes followed by fusion of the agglomerated system. The layering is induced by a cooperative bridging of bilayers via adsorbed R_9. The peptides also induce membrane bifurcations that allow us to connect the vesicle exterior and interior via fusion and thus to translocate the CPPs (which would not be topologically possible within an ideal vesicle fusion). The actual R_9-induced fusion process then mirrors that of Ca^{2+}-assisted vesicle fusion. The viability of this mechanism is supported by experimental results from EM, fluorescence microscopy, and light scattering, together with with molecular dynamics simulations. The atomistic simulation data shed further light on the molecular mechanism of formation of the fusion stalk and pore. While this mechanism has been unraveled for lipid vesicle systems, which allow for investigations with unprecedented molecular detail, induction of membrane branching and multilamellarity by polyarginines has been observed by EM also in cellular membranes of live cells at low temperatures, indicating that the passive cell penetration process analogously involves membrane fusion.

Future work will be directed toward unraveling further molecular details of the cell penetration mechanism suggested in this discovery study. In the next step, we need to understand the interaction of CPPs with biological cell surfaces. Increased experimental understanding of the specific binding will allow us to develop more realistic models and vice versa. This will not only allow us to firmly establish all of the details of this hithertho unrecognized mechanism of passive cell penetration, but also have a direct impact on development of smart cell delivery strategies for therapeutic molecules using CPPs. Should we get this passive cell penetration mechanism under full control, we may eventually be able to exploit it to directly deliver cargo into the cell without the need for releasing it from the transport vesicles, as is the case in active endocytosis.

Materials and Methods

Liposome Experiments.

Leakage. Calcein-containing vesicles were stirred at room temperature with LUV buffer in a quartz cuvette to obtain 1.5 mL of solution. The calcein fluorescence was monitored at 520 nm, with excitation at 495 nm. After an initial stirring phase of no less than 200 s, 3–6 μL peptide in buffer solution was added. After the fluorescence intensity reached a plateau, 50 μL of TRITON-X was added. Fluorescence intensity measurements were performed on a Fluorolog-3 spectrofluorimeter (model FL3–11; JobinYvon Inc.) equipped with a xenon-arc lamp. See *SI Appendix* for further details.

Confocal microscopy. GUVs labeled with DiD were prepared for confocal microscopy using electroformation in a 300-mOsm/L sucrose solution. Prepared GUVs were diluted with a glucose buffer [9 mM HEPES, pH 7.40 (KOH), 90 mM KCl, 90 mM EDTA, 120 mM glucose, 300 mOsm/L, filtrated] with 20 μL of 50 nM Atto 488 to a total volume of 300 μL. Images were recorded using an Olympus IX81 laser scanning confocal microscope. For further details see *SI Appendix*.

Cryo-EM. For cryo-EM sample preparation, 4 μL of the sample was applied to plasma-cleaned EM grids [400-mesh copper grids, covered with Quantifoil film (R1.2/1.3)]. Samples were plunge frozen on the grids in liquid ethane in a Grid Plunger (Leica EM GP; Leica Microsystems GmbH) with the following parameters: preblotting exposure 5 s, blotting time 1.7 s, no postblotting exposure. Chamber humidity was set to 95% at 22 °C. The LUV solution was treated with R_9 (c = 25 mM) in a ratio of 10:1 for $t > 60$ s immediately before plunge freezing. Cryoelectron micrographs were collected on a JEM-2100F (JEOL Germany GmbH) operated at 200 kV (see *SI Appendix* for further details).

Cell Experiments. Forty thousand HeLa cells were seeded to a well of μ-slide (ibiTreat; ibidi) 16–20 h before the experiment. Cells were washed with SF-DMEM and kept at 4 °C for 15 min to inhibit endocytic processes. For treatment, a precooled (4 °C) 15-μM solution of a peptide in SF-DMEM was added to cells via media exchange and incubated for indicated periods of time at 4 °C. In selected cases, cells were treated for 3 min with a peptide at 4 °C, washed with precooled SF-DMEM, and further incubated for an indicated period at 4 °C in fresh SF-DMEM. Cells were imaged using a scanning confocal microscope (FluoView 1000; Olympus) and the tomograms were acquired on a Titan Halo transmission electron microscope (see *SI Appendix* for details).

Computational Details. We use all atom molecular dynamics (MD) for the fusion process: In a first setup, we created two curved membranes via lipid population imbalances at the two leaflets of each bilayer. In the second setup, we put a very small vesicle composed of DOPE (80%) and DOPS (20%) in the unit cell and let it fuse with its periodic image. Both of these approaches facilitate formation of the stalk without enforcing its shape. For calcium fusion we used optimized charge-scaled force fields for ions, to account effectively for electronic polarization effects. For vesicle aggregation and bifurcation calculations we used coarse-graining methods. See *SI Appendix* for full details.

ACKNOWLEDGMENTS. We thank Aleš Bendar, Markéta Dalecká, Mario Vazdar, Daniel Harries, Šárka Pokorná, Uri Raviv, and Lea Fink for discussions and technical assistance. P. Jungwirth acknowledges support from the Czech Science Foundation (Grant 16-01074S). C.A. thanks the German Academic Exchange Service for support via a Prime fellowship and the Minerva foundation for a postdoctoral fellowship. A.M. acknowledges the Magnus Ehrnrooth Foundation, Finland for funding. R.S. and M.H. acknowledge the Czech Science Foundation (Grant 17-03160S). Allocation of computer time from the Finnish IT Center for Science (CSC) is appreciated. V.H., R.R.,

and C.M.Z. acknowledge the use of the cryoelectron microscope in the Department of Molecular Cell Anatomy, University of Regensburg, headed by Ralph Witzgall. We acknowledge the Imaging Methods Core Facility at BIOCEV, Faculty of Sciences, Charles University, an institution supported by the Czech-BioImaging large research infrastructure project (LM2015062 and CZ.02.1.01/0.0/0.0/16_013/0001775 funded by the Czech Ministry of Education), for their support with obtaining imaging data presented in this paper.

1. Bechara C, Sagan S (2013) Cell-penetrating peptides: 20 years later, where do we stand? *FEBS Lett* 587:1693–1702.
2. Wadia JS, Stan RV, Dowdy SF (2004) Transducible TAT-HA fusogenic peptide enhances escape of TAT-fusion proteins after lipid raft macropinocytosis. *Nat Med* 10:310–315.
3. Pae J, et al. (2014) Translocation of cell-penetrating peptides across the plasma membrane is controlled by cholesterol and microenvironment created by membranous proteins. *J Control Release* 192:103–113.
4. Mishra A, et al. (2011) Translocation of HIV TAT peptide and analogues induced by multiplexed membrane and cytoskeletal interactions. *Proc Natl Acad Sci USA* 108:16883–16888.
5. Lamazière A, et al. (2007) Non-metabolic membrane tubulation and permeability induced by bioactive peptides. *PLoS One* 2:e201.
6. Sun D, Forsman J, Lund M, Woodward CE (2014) Effect of arginine-rich cell penetrating peptides on membrane pore formation and life-times: A molecular simulation study. *Phys Chem Chem Phys* 16:20785–20795.
7. Herce HD, Garcia AE, Cardoso MC (2014) Fundamental molecular mechanism for the cellular uptake of guanidinium-rich molecules. *J Am Chem Soc* 136:17459–17467.
8. Ciobanasu C, Siebrasse JP, Kubitscheck U (2010) Cell-penetrating HIV1 TAT peptides can generate pores in model membranes. *Biophys J* 99:153–162.
9. Zasloff M (2002) Antimicrobial peptides of multicellular organisms. *Nature* 415:389–395.
10. Lee MT, Sun TL, Hung WC, Huang HW (2013) Process of inducing pores in membranes by melittin. *Proc Natl Acad Sci USA* 110:14243–14248.
11. Marks JR, Placone J, Hristova K, Wimley WC (2011) Spontaneous membrane-translocating peptides by orthogonal high-throughput screening. *J Am Chem Soc* 133:8995–9004.
12. Guterstam P, et al. (2009) Elucidating cell-penetrating peptide mechanisms of action for membrane interaction, cellular uptake, and translocation utilizing the hydrophobic counter-anion pyrenebutyrate. *Biochim Biophys Acta Biomembr* 1788:2509–2517.
13. Maniti O, Piao HR, Ayala-Sanmartin J (2014) Basic cell penetrating peptides induce plasma membrane positive curvature, lipid domain separation and protein redistribution. *Int J Biochem Cell Biol* 50:73–81.
14. Swiecicki JM, et al. (2015) Accumulation of cell-penetrating peptides in large unilamellar vesicles: A straightforward screening assay for investigating the internalization mechanism. *Pept Sci* 104:533–543.
15. Katayama S, et al. (2013) Effects of pyrenebutyrate on the translocation of arginine-rich cell-penetrating peptides through artificial membranes: Recruiting peptides to the membranes, dissipating liquid-ordered phases, and inducing curvature. *Biochim Biophys Acta Biomembr* 1828:2134–2142.
16. Gestin M, Dowaidar M, Langel Ü (2017) *Uptake Mechanism of Cell-Penetrating Peptides*, eds Sunna A, Care A, Bergquist PL (Springer International Publishing, Cham, Switzerland), pp 255–264.
17. Chen YA, Scheller RH (2001) Snare-mediated membrane fusion. *Nat Rev Mol Cell Biol* 2:98–106.
18. Chen YA, Scales SJ, Patel SM, Doung YC, Scheller RH (1999) SNARE complex formation is triggered by Ca2+ and drives membrane fusion. *Cell* 97:165–174.
19. Babai N, Kochubey O, Keller D, Schneggenburger R (2014) An alien divalent ion reveals a major role for Ca2+ buffering in controlling slow transmitter release. *J Neurosci* 34:12622–12635.
20. Papahadjopoulos D, Vail W, Pangborn W, Poste G (1976) Studies on membrane fusion. II. Induction of fusion in pure phospholipid membranes by calcium ions and other divalent metals. *Biochim Biophys Acta* 448:265–283.
21. Brock TG, Nagaprakash K, Margolis DI, Smolen JE (1994) Modeling degranulation with liposomes: Effect of lipid composition on membrane fusion. *J Memb Biol* 141:139–148.
22. Schneggenburger R, Rosenmund C (2015) Molecular mechanisms governing Ca2+ regulation of evoked and spontaneous release. *Nat Neurosci* 18:935–941.
23. Kozlovsky Y, Kozlov MM (2002) Stalk model of membrane fusion: Solution of energy crisis. *Biophys J* 82:882–895.
24. Zhao WD, et al. (2016) Hemi-fused structure mediates and controls fusion and fission in live cells. *Nature* 534:548–552.
25. Yang ST, Zaitseva E, Chernomordik LV, Melikov K (2010) Cell-penetrating peptide induces leaky fusion of liposomes containing late endosome-specific anionic lipid. *Biophys J* 99:2525–2533.
26. Tünnemann G, et al. (2008) Live-cell analysis of cell penetration ability and toxicity of oligo-arginines. *J Pept Sci* 14:469–476.
27. Mitchell D, Steinman L, Kim D, Fathman C, Rothbard J (2000) Polyarginine enters cells more efficiently than other polycationic homopolymers. *J Pept Res* 56:318–325.
28. Hu Y, Sinha SK, Patel S (2015) Investigating hydrophilic pores in model lipid bilayers using molecular simulations: Correlating bilayer properties with pore-formation thermodynamics. *Langmuir* 31:6615–6631.
29. Churchward MA, et al. (2008) Specific lipids supply critical negative spontaneous curvature—an essential component of native Ca2+-triggered membrane fusion. *Biophys J* 94:3976–3986.
30. Düzgünes N, Wilschut J, Fraley R, Papahadjopoulos D (1981) Studies on the mechanism of membrane fusion. Role of head-group composition in calcium- and magnesium-induced fusion of mixed phospholipid vesicles. *Biochim Biophys Acta* 642:182–195.
31. Summers SA, Guebert BA, Shanahan MF (1996) Polyphosphoinositide inclusion in artificial lipid bilayer vesicles promotes divalent cation-dependent membrane fusion. *Biophys J* 71:3199–3206.
32. Churchward MA, et al. (2008) Specific lipids supply critical negative spontaneous curvature—an essential component of native Ca2+-triggered membrane fusion. *Biophys. J* 94:3976–3986.
33. Kachar B, Fuller N, Rand R (1986) Morphological responses to calcium-induced interaction of phosphatidylserine-containing vesicles. *Biophys J* 50:779–788.
34. Grafmüller A, Shillcock J, Lipowsky R (2007) Pathway of membrane fusion with two tension-dependent energy barriers. *Phys Rev Lett* 98:218101.
35. Marrink SJ, Mark AE (2003) The mechanism of vesicle fusion as revealed by molecular dynamics simulations. *J Am Chem Soc* 125:11144–11145.
36. Noguchi H, Takasu M (2001) Fusion pathways of vesicles: A Brownian dynamics simulation. *J Chem Phys* 115:9547–9551.
37. Fuhrmans M, Marrink SJ (2012) Molecular view of the role of fusion peptides in promoting positive membrane curvature. *J Am Chem Soc* 134:1543–1552.
38. Derossi D, et al. (1996) Cell internalization of the third helix of the antennapedia homeodomain is receptor-independent. *J Biol Chem* 271:18188–18193.
39. Kawamoto S, et al. (2011) Inverted micelle formation of cell-penetrating peptide studied by coarse-grained simulation: Importance of attractive force between cell-penetrating peptides and lipid head group. *J Chem Phys* 134:095103.
40. Siegel DP, Kozlov MM (2004) The Gaussian curvature elastic modulus of N-monomethylated dioleoylphosphatidylethanolamine: Relevance to membrane fusion and lipid phase behavior. *Biophys J* 87:366–374.
41. Hirose H, et al. (2012) Transient focal membrane deformation induced by arginine-rich peptides leads to their direct penetration into cells. *Mol Ther* 20:984–993.
42. Kawamoto S, Klein ML, Shinoda W (2015) Coarse-grained molecular dynamics study of membrane fusion: Curvature effects on free energy barriers along the stalk mechanism. *J Chem Phys* 143:243112.
43. Nir S, Wilschut J, Bentz J (1982) The rate of fusion of phospholipid vesicles and the role of bilayer curvature. *Biochim Biophys Acta* 688:275–278.
44. Robison AD, et al. (2016) Polyarginine interacts more strongly and cooperatively than polylysine with phospholipid bilayers. *J Phys Chem B* 120:9287–9296.
45. Allolio C, Haluts A, Harries D (2018) A local instantaneous surface method for extracting membrane elastic moduli from simulation: Comparison with other strategies. *Chem Phys*, 10.1016/j.chemphys.2018.03.004.